59th ILMENAU SCIENTIFIC COLLOQUIUM
Technische Universität Ilmenau, 11 – 15 September 2017
URN: urn:nbn:de:gbv:ilm1-2017iwk-005:6

SCREW-DRIVEN ROBOT FOR LOCOMOTION INTO SAND

Roy Lichtenheldt[1], *Felix Becker*[2], *Klaus Zimmermann*[2]

[1]German Aerospace Center (DLR), Robotics and Mechatronics Center
[2]Technische Universität Ilmenau, Technical Mechanics Group

ABSTRACT

The locomotion into sand is needed in various applications, but due to the complex mechanics of granular matter it causes special difficulties. High resistance forces on penetration systems and parameter dependent behavior, like stable or instable boreholes, complicate the design of mobile robots for the locomotion in sandy soil. The most effective state of the art devices deploy hammering mechanisms. Screw-driven systems arise more and more in the literature, as they promise to be a simple, robust and low-cost solution. In this paper, an autonomous drilling robot for the locomotion into sandy soils is presented. The design is based on theoretical modeling and experimental analyses of the screw drive aiming to minimize the needed torque and to maximize the locomotion speed. The presented prototype is able to reach a depth of 20 centimeters within a minute with a torque of 0.66 Nm.

Index Terms **–** Mobile robot, locomotion, sand, granular matter, screw drive

1. INTRODUCTION

Wherever risks for human operators are high, or the areas are inaccessible at all, autonomous robots are able to support the exploration of the mentioned areas. The use of soil penetration systems ranges from everyday terrestrial applications like trenchless pipe and cable laying over disaster management to tasks like planetary subsurface exploration.
The mechanics of granular matters is still not fully understood. Its complex micromechanical behavior causes special effects on macroscopic scale. Thus, locomotion into sands is complicated by effects like the conditional liquidification dependent on the load history. Due to the solid phase in subcritical loading, high resistance forces on locomotion systems are arising, and boreholes might be open or collapse dependent on soil parameters. Furthermore, granular matter is abrasive by nature, and thus poses a threat to every technical system it ingresses. To avoid excessive wear and early end of life, the sealing concept is a major part of the design of subsurface locomotion systems.
In order to tackle those difficulties, we developed an autonomous, low-cost drilling robot with internal energy supply. The design has been model-based with the aim to lower the number of needed prototypes to be operational. As the purpose is to gain optimal locomotion performance as well as low energy consumption, the screw geometry is varied and tested. A special testbed has been set up to perform systematic measurements, varying the screw's geometric parameters. The prototype is tested in different soils: quartz sand, chalk and lava sand.

2. STATE OF THE ART

The most established principles to autonomously explore the subsurface of sandy sediments are internal hammering mechanisms [1-6]. To cite an example, the NASA InSight mission,

planned to launch in May 2018, will feature a self-impelling nail nicknamed the "Mole" to transport heat sensors five meters into the sandy Martian regolith [5-6]. So far hammering is the only principle capable of reaching depth greater than several body lengths of the systems. Due to the incremental, periodic strokes, energy consumption is kept low while still achieving high locomotion performance. But these positive effects come with the cost of high inner shock loads, which cause high development costs. Furthermore, complex simulations and optimization runs are required to cover the inner dynamics and to design properly the mechanism [5].
In comparison to the high technical readiness level of autonomous hammering devices, the state of the art drilling systems are primarily in early prototype states. Most of those robots do not reach depth much higher than their own body length, cf. Fig. 1 [7-10]. The effect is not yet fully understood, but the most prominent reason mentioned is the limited actuation torque in relation to the high soil resistance. There are only few attempts to understand the cause of immobilization by modeling, such as in [8].
Alternative designs, such as the combination of different motion principles, are reported in the literature [11-14]. The robot shown in [11-12] is using combined hammering and drilling, but requires a stable open borehole. Deploying several screws, [15] presents a robot able to roll and drill. Additionally, biologically inspired systems are also reported in literature [16-22].

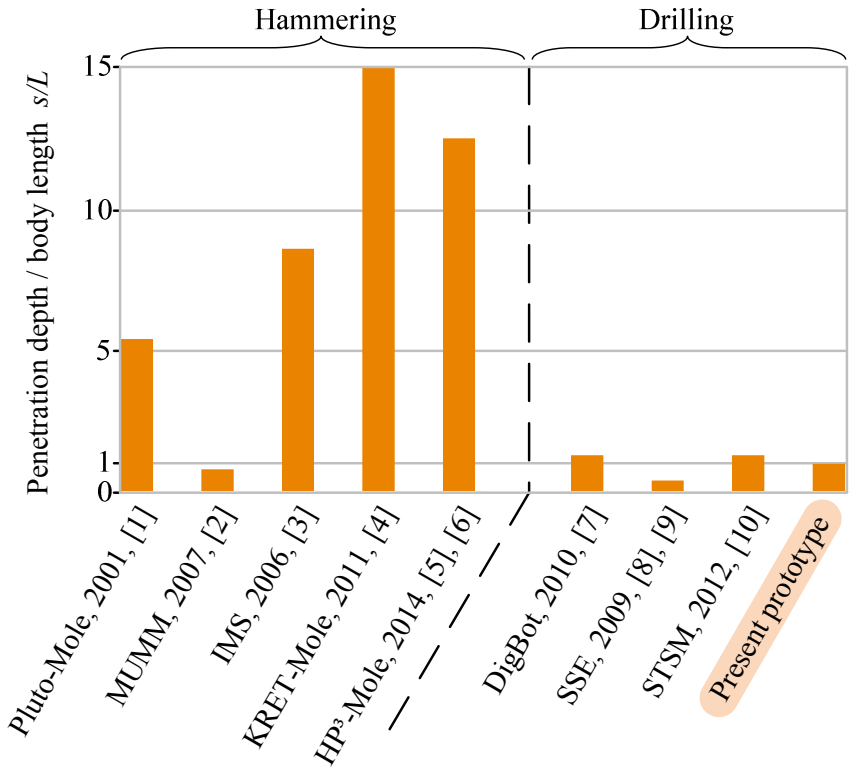

Figure 1: State of the art prototypes compared by the ratio of penetration depth and body length s/L.

3. MODELING

Modeling and simulation in this field is mainly divided into two streams: complex, high-fidelity numerical models and simpler, but faster, analytical and empirical models. High-fidelity models are often based on Finite [23-24] or Discrete Element Method [5, 25]. Even though those models are adequate to the real system on a specified abstraction level, they are not fast enough for quick engineering decisions. Faster models are mostly based on RANKINE's theory of earth pressure or empirical equations. Such approaches are shown by

[6, 8, 26]. Following, a simple model for fast approximations in sub-surface robot design will be derived.
As shown in Fig. 2 (a), the forces are divided into resistive F_S, F_R and propulsive forces F_A. Thereby resistance is mainly caused by the frictional force on the outer shell F_R and the tip resistance $F_S = Aq_S$. The aim for the engineering model of the screw-driven robot is to gather a quasi-static description of the forces acting on its body. To cover the frictional forces, RANKINE'S soil pressure [27] is applied as in [8, 26] in order to calculate the horizontal stress, cf. Fig. 2 (b):

$$\sigma_h = \rho_s g K z + qK + 2c\sqrt{K}, \tag{1}$$

with ρ_s the soil bulk density, K the soil pressure coefficient, q the surcharge and c the soil cohesion. Thus, the horizontal force derives to:

$$\vec{F}_h = \vec{e}_r \int\int \left(\rho_s g K z + qK + 2c\sqrt{K}\right) dA, \tag{2}$$

$$\vec{F}_h = \vec{e}_r \left(\int_0^{2\pi} \int_{s_0}^{s} \sigma_h \, R dz \, d\varphi\right);\ s_0 = \begin{cases} 0; & \forall\, s \le L \\ (s-L) & ;\forall\, s > L \end{cases} \tag{3}$$

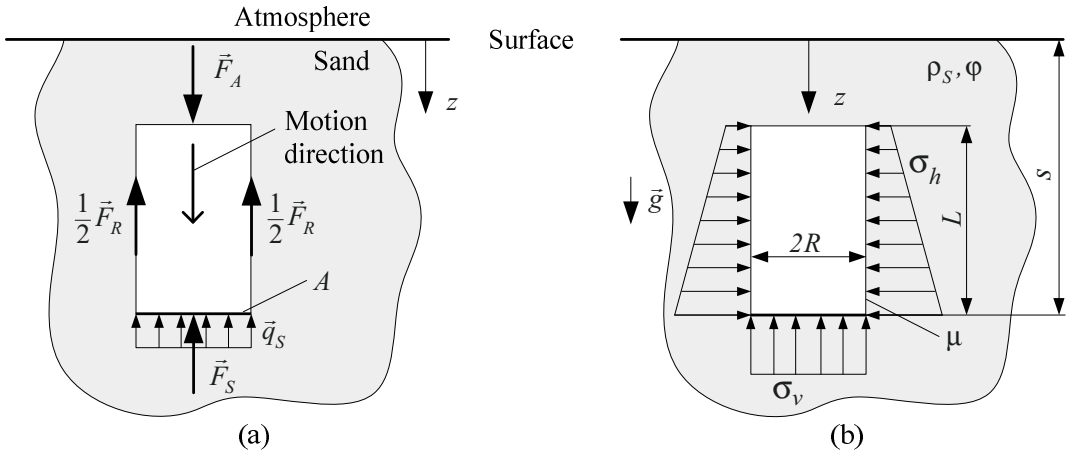

Figure 2: (a) *– Forces on the body moving vertically into granular matter:* $\vec{F}_A$ *- actuation force,* $\vec{F}_R$ *- friction force,* $\vec{F}_S = A\vec{q}_S$ *- ground resistance force, A - cross sectional area,* $\vec{q}_S$ *- resistive pressure;* (b) *– Model of the soil pressure: R – radius, L - length, s - depth,* μ *- friction coefficient,* $\vec{g}$ *- gravitation acceleration,* σ_h, σ_v *- horizontal, vertical soil pressure,* ρ_S *- bulk density,* φ *- friction angle.*

The adaption by [26] to cover soil cohesion for penetration devices is used. The line load f_h derives to:

$$\vec{f}_h = \vec{e}_r \begin{cases} \frac{1}{2}\gamma_s K s^2 + \left(qK - c\,\frac{v_z}{|v_z|}\sqrt{K}\right)\cdot s; & \forall s \le L \\ \left(s - \frac{L}{2}\right)\gamma_s L K + (s-L)\left(qK - c\,\frac{v_z}{|v_z|}\sqrt{K}\right); & \forall s > L \end{cases} \tag{4}$$

with v_z the robots velocity in z direction and the gravitational weight $\gamma_s = \rho_s g$ of the soil. By the motion of the robot into the soil, a cavity needs to be opened. The opening of this enclosing cavity causes a soil displacement, which may be treated as a virtual wall movement Δr in direction of $\vec{e}_r$. The soil pressure coefficient is, cf. [27]:

$$K(\varphi,\Delta r)=\begin{cases}\tan^2\left(\frac{\pi}{4}-\varphi\right); & \forall\,\Delta r\ \le -0.001\cdot s\\ 1-\sin(\varphi); & \forall\,\Delta r\ \approx 0\cdot s\\ \tan^2\left(\frac{\pi}{4}+\varphi\right); & \forall\,\Delta r\ \ge 0.05\cdot s\end{cases} \quad (6)$$

As the cavity in the soil is opened by the robots tip, no virtual wall movement at the outer hull can be assumed. The soil pressure coefficient K simplifies to the soil pressure K_0 at rest, cf. [28]:

$$K = K_0 = 1-\sin(\varphi) \quad (7)$$

Applying f_N to Coulomb's friction for slipping and stiction as shown in [26] yields:

$$\vec{F}_R = 2\pi R\frac{v_z}{|v_z|}\vec{e}_\gamma \times \vec{f}_h\begin{cases}\tan(\varphi_\mathrm{H}); & \forall\, v_z < v_r\\ \tan(\varphi_\mathrm{G}); & \forall\, v_z \ge v_r\end{cases} \quad (8)$$

whereby φ_H and φ_G are the stiction and slipping interface friction angles, $\vec{e}_\gamma$ the tangential component of the cylinder coordinates and v_r the friction dead band velocity.
Due to the assumption that the cavity enclosing the robot is opened by its tip, an additional force is needed to cover this effect. In literature this force is covered by empirical models, e.g., an elasto-plastic element [26], soil pressure or by cavity expansion theory (CET) [6,8]. CET is based on the energy needed to open the cavity inside the soil [29-30]. The approach assumes several deformation zones around the penetrating body: plastic zone, non-linear elastic and elastic zone. By application of the simplified empirical CET, a prediction accuracy of $\pm 40\%$ is stated. Utilizing it for the sand screw tip, it yields:

$$\vec{F}_S = 5.15\cdot R^2\cdot p_A\cdot e^{(0.1041\varphi+(0.0264-0.0002\varphi)\rho_r)}\cdot\left(\frac{K_0 gs}{p_A}\right)^{(0.841-0.0047)\rho_r}\cdot\vec{e}_z;\quad \forall\,\varphi\in[0.506,0.628] \quad (9)$$

which means for friction angles between 29° and 36°. p_A is the unit pressure. With all the resistive forces covered as shown above, the propellent force is derived by the soil weight on top of the robot and the driving force $\vec{F}_D$ of the screw:

$$\vec{F}_A = g\vec{e}_z(\rho_s(z-L)A+m_R)+\vec{F}_D \quad (10)$$

with m_R the robots mass. It should be noted that the literature does not sufficiently cover $\vec{F}_D$. E.g., [8] gives an estimate dependent on the slip of the device, which itself depends on the propellent and resistive forces as well as the exerted torque. Given the open issues in driving force models, this part of the model will be subject to ongoing research. The models have been used in the development of the robot, to predict the behaviour before the first prototype has been available.
In order to verify the proposed force models, dedicated measurements have been performed. Throughout the tests a nearly cohesionless quartz sand, similar to the Martian simulant used for the HP³ [26], is used. The parameters are:

$$\rho_\mathrm{s} = 1600\ \mathrm{kg/m^3};\quad \varphi = 31°;\quad c \ll 1\ \mathrm{kPa}.$$

To measure the frictional forces, a cone indenter is equipped with a hollow cylinder and embedded into the soil in different depths up to 450 mm. The force needed for extracting the hollow cylinder is measured. To verify the further complex interaction at the tip, cylindrical

as well as conical indenter have been loaded with weights of 10 – 25 kg and the resultant penetration depth is measured. Fig. 3 shows the results of the campaign. For all the cylindrical indenters the prediction using the CET is in good correlation with the measurements. The conical indenters however show the expected lower resistance values over depth, which are right near the lower boundary of the ±40% confidence interval.

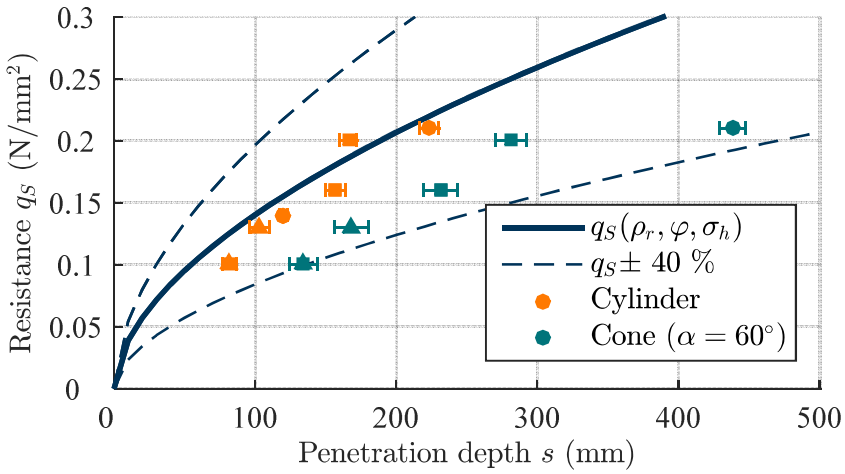

Figure 3: Analytic and experimental results of the front resistance $q_S = F_S/A$ of cylindrical bodies and conical bodies with the cone angle α = 60°: ●- Ø 30 mm, ■- Ø 40 mm, ▲- Ø 50 mm..

As worst-case estimates are needed in order to develop robots for harsh environments, the CET is still a valid worst-case approximation of the tip resistance. As the CET also does not directly pose a dependency on the tip's cone angle α, the dependency of the tip resistance q against the cone angle is measured analog to the CET verification. In Fig. 4 it can be seen that a minimum in cone resistance occurs at α = 40°. For lower angles, the resistance is slightly increasing again. This result coincides with the findings of Whitaker 1976 [31]. Absolute differences may be explained by differences in the used soil. The comparison of the result to [32] shows good correlation for the pure cone resistance, substracting frictional forces, too.

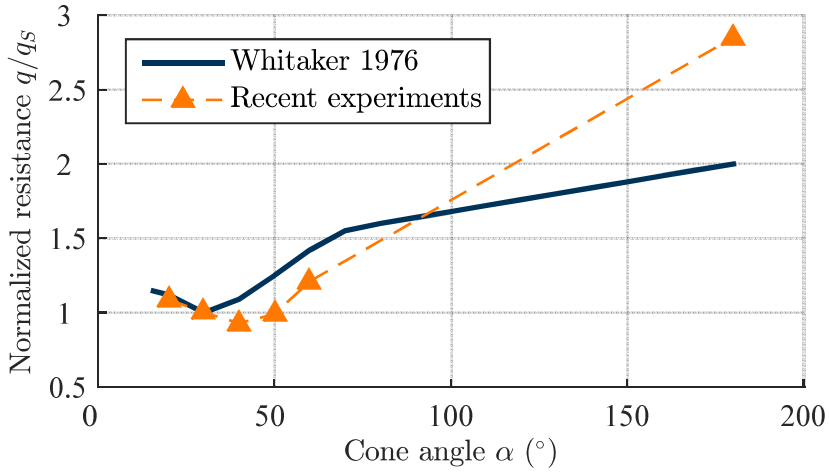

Figure 4: Experimentally obtained resistance values normalized to the cone angle of α = 30°.

Using the proposed model, it is possible to predict the forces on the robot and to size certain parts. As the quasi-static approach still poses several limitations and the CET tends to overestimate the resistive forces, a fully dynamic model with enhanced force description is subject to future research.

4. EXPERIMENTS

The critical part of a drilling robot is the screw drive, which is used to create a translational motion from the rotational motor. As the locomotion is highly dependent on the parameters of the screw drive, a testbed to investigate the influences has been developed. The testbed for the experimental invesitgations is presented in Fig. 5. The aim is to find an effective and efficient screw design. While the screw samples are drilled into the sand, the penetration depth, torque and rotaional and translational speed are measured simultaneously.

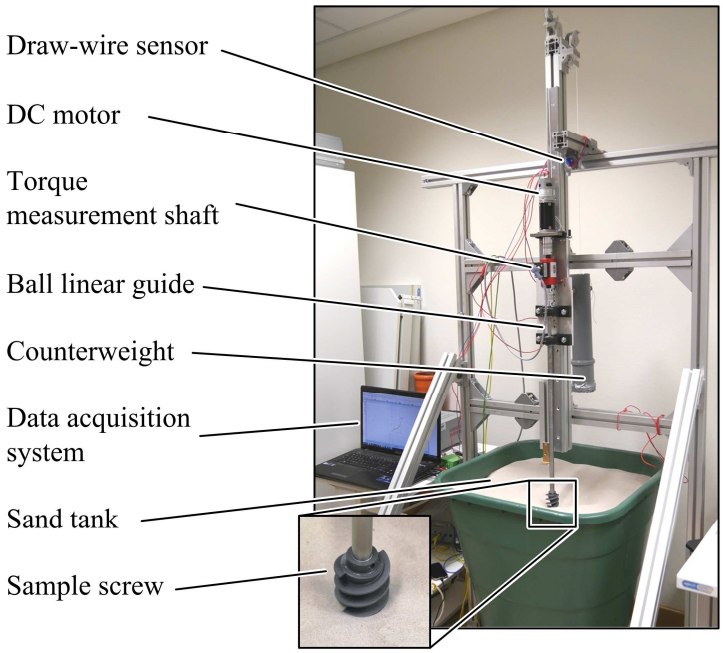

Figure 5: Testbed for the experimental validation of the screw samples.

The sand tank is 70 cm in height and has an average diameter of 50 cm. The soil simulant used is a quartz sand of around 98 % SiO_2. The sand contains no grains bigger than 2000 µm and more than 80 % of the grains are sized between 200 µm and 1500 µm. A similar sand is used in [26] as reference Martian simulant. Additionally, quartz sand is only weakly hygroscopic enabling to neglect effects by cohesion due to the humidity of the laboratory air (average: 32 %). In order to achieve comparable test results, it is important to gain comparable soil states throughout consecutive measurements. Therefore, the sand is loosened up inbetween the single measurements to avoid compaction by experiments or settling.
The screwhead is driven by a DC motor producing up to 10 Nm of torque. This provides sufficient torque to avoid immobilization due to resistance torques and to achieve a shaft speed of 8.8 rpm. A constant vertical force of F_A = 6.2 N is applied. In order to measure the torque M, the penetration depth s and the translational speed v, a torque measurement shaft and a draw-wire sensor are used. The analogue and digital sensor signals are recorded simultaneously using a DAQ hardware and software by National Instruments.
For the measurements, screws with both right-handed (Type 1, grey color) and left-handed threads (Type 2, blue color) are used. Type 1 has a conical core, while the core of Type 2 is formed by a cylinder with a conical tip and bottom. The schematics of the screws showing their parameterization are presented in Fig. 6. The screw samples are produced by additive rapid prototyping. The used polylactide is postprocessed by chemical smoothing using dichloromethane after printing. The parameters of the screws are given in Tab. 1. The

experimental results are shown in Fig. 7 and Fig. 8. The mean values (MV) of five repetitions for each sample are plotted as a continuous line.

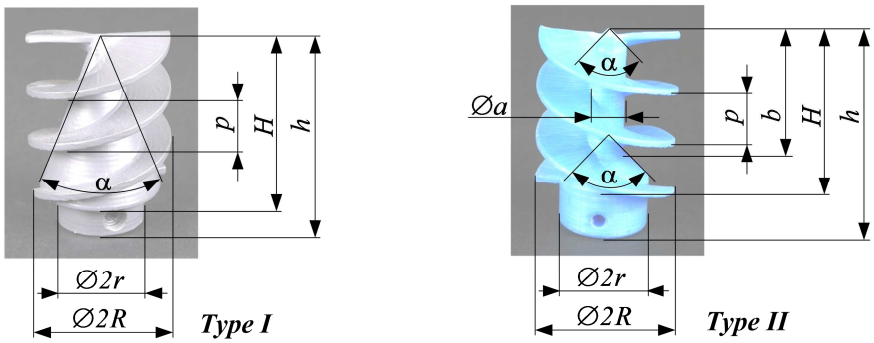

Figure 6: Schematic screws with characteristic parameters.

Table 1: Parameters of experimental screw samples.

Parameters		**Screw samples**	
Term	***Symbol (Unit)***	***Type I***	***Type II***
Thread radius	R (mm)	20; 22.5; 25	10; 13.5; 20
Thread height	H (mm)	46	46; 90
Pitch	p (mm)	15; 22.5	15; 22.5
Cone angle	α (°)	40	45
Core radius	a (mm)	-	5
Bottom radius	r (mm)	17	17
Cone height	b (mm)	-	36; 82
Total height	h (mm)	56	56; 104
Thread		Right-handed	Left-handed

The dashed lines, the filled area between the curves in Fig. 7 and the lighter bars in Fig. 8 represent the root mean square (RMS) deviation, calculated by MV ± RMS.
The maximum depth of each screw results from the vertical limits of the experimental setup and the screw height h. It is obvious that the required torque M and the translational velocity v depend on the penetration depth s and screw parameters. Fig. 7 and Fig. 8 show that screw samples with small thread radius are not able to reach greater depth. The applied torque cannot be transferred to the soil and the screws rotate without translational progress. However, too large radii R lead to disadvantageous effects. The required torque increases, and the achievable speed decreases.
Comparing the two different screw types it can be obtained that the samples of Type 2 with the smaller, cylindrical core are faster and need less torque than Type 1 with the larger, conical core. As presented in Fig. 8, the modification of the thread pitch has a remarkable influence on the torque M, and the time t that a screw needs to reach a certain depth. The increase of the pitch leads to faster translational motion and the need of higher torques.

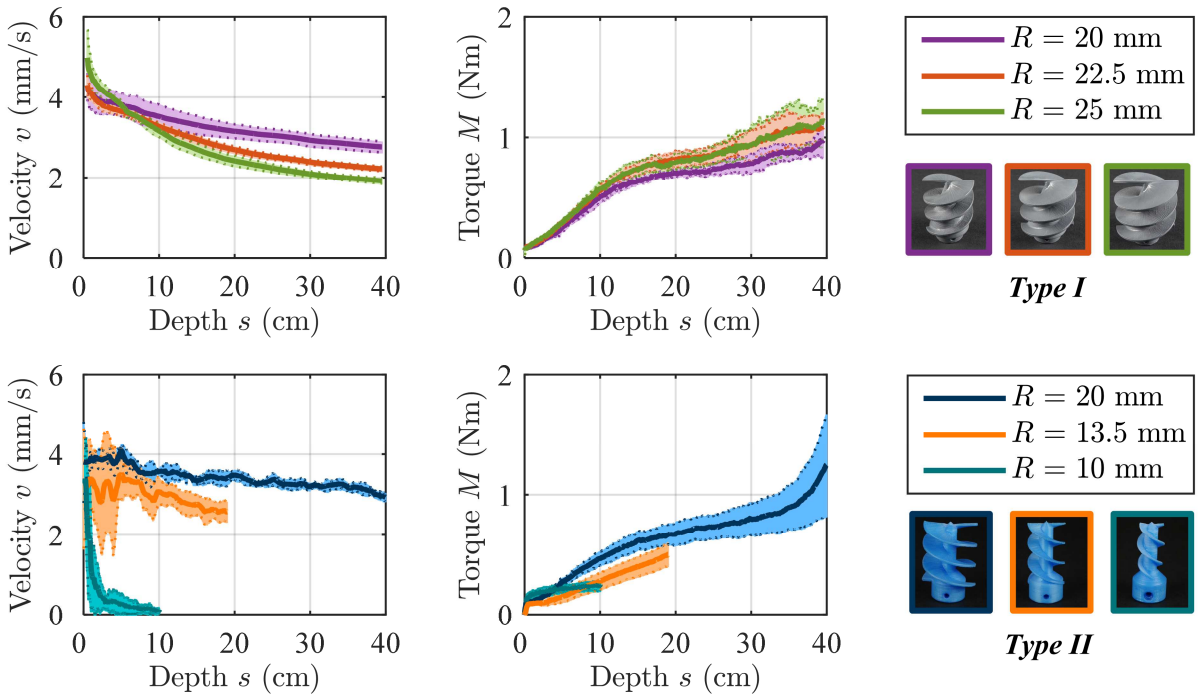

Figure 7: Velocity v and torque M against depth s dependent on the radius R of the screw thread.

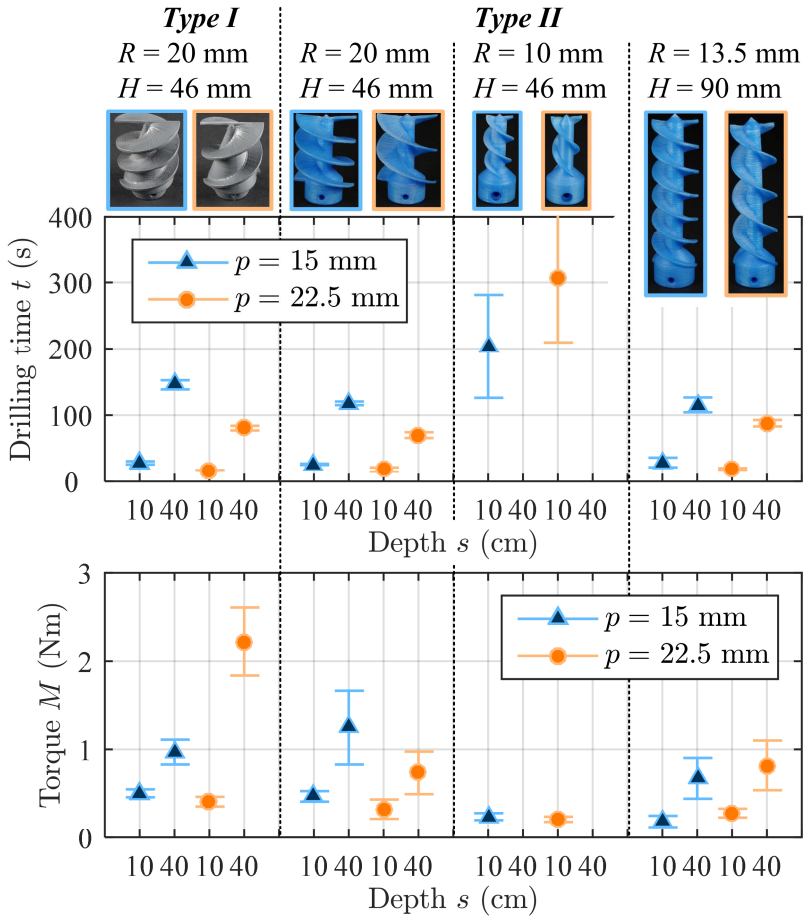

Figure 8: Drilling time t and torque M in depth s of 10 cm and 40 cm dependent on the pitch p of different screw types.

5. ROBOT

For the design of the full robot, a single screw had to be chosen. A compromise between locomotion performance, i.e. high average speed, and energy consumption, i.e. low maximum torque, was made. The Type 1 screw with the best performance (purple graphs in Fig. 7, $R = 20$ mm) is used. The developed robot was first described in [33]. Characteristic parameters are given in Tab. 2. The exploded view of CAD-design is presented in Fig. 9. The prototype is driven by a DC motor with an epicyclic gearing. For autonomous operation, energy is supplied by a lithium-ion battery. The current is limited electronically to 0.5 A in order to reduce heating. Using this current limit, a torque of 0.66 Nm is achieved. With this setup, the robot reaches a depth of 20 cm in less than a minute, see Fig. 10.

Table 2: Characteristic parameters of the battery-powered robot prototype.

Diameter (main cylinder)	D (mm)	28
Span (anti-torque panels)	S (mm)	81
Length (with sample screw)	L (mm)	204
Mass	m (g)	150
Angular velocity	N (rpm)	11
Maximal torque	M (Nm)	0.66
Maximal depth	s (cm)	20
Translational velocity	v (mm/s)	4.6
Operation time (with 800 mAh battery)	T (min)	57

As the robot features external parts with relative rotation, the interface needs to be properly sealed. Therefore, a two-staged sealing concept using rotational symmetric silicone seals is chosen. The first stage is V-seal followed by second stage radial shaft seal. The inter-sealing space is filled with grease to trap particles that may pass the V-seal. This concept was successfully tested in several soils and showed no sand ingress on the internals of the robot.
In order to verify the principle, the robot has also been tested in two further Martian soil simulants in the Planetary Exploration Laboratory at German Aerospace Center. Thereby it was possible to show that the system is also able to proceed into coarse grained, gravelly lava sands as well as very fine cohesive simulants without much impact on performance, as it is presented in Fig. 10.
While conducting those tests higher than nominal motor currents are tested as well. At higher motor current the immobilization is not necessarily caused by stopping of the screw rotation. A second failure mode caused by insufficient soil strength at the screw head was discovered, causing the screw to spin freely in the soil.

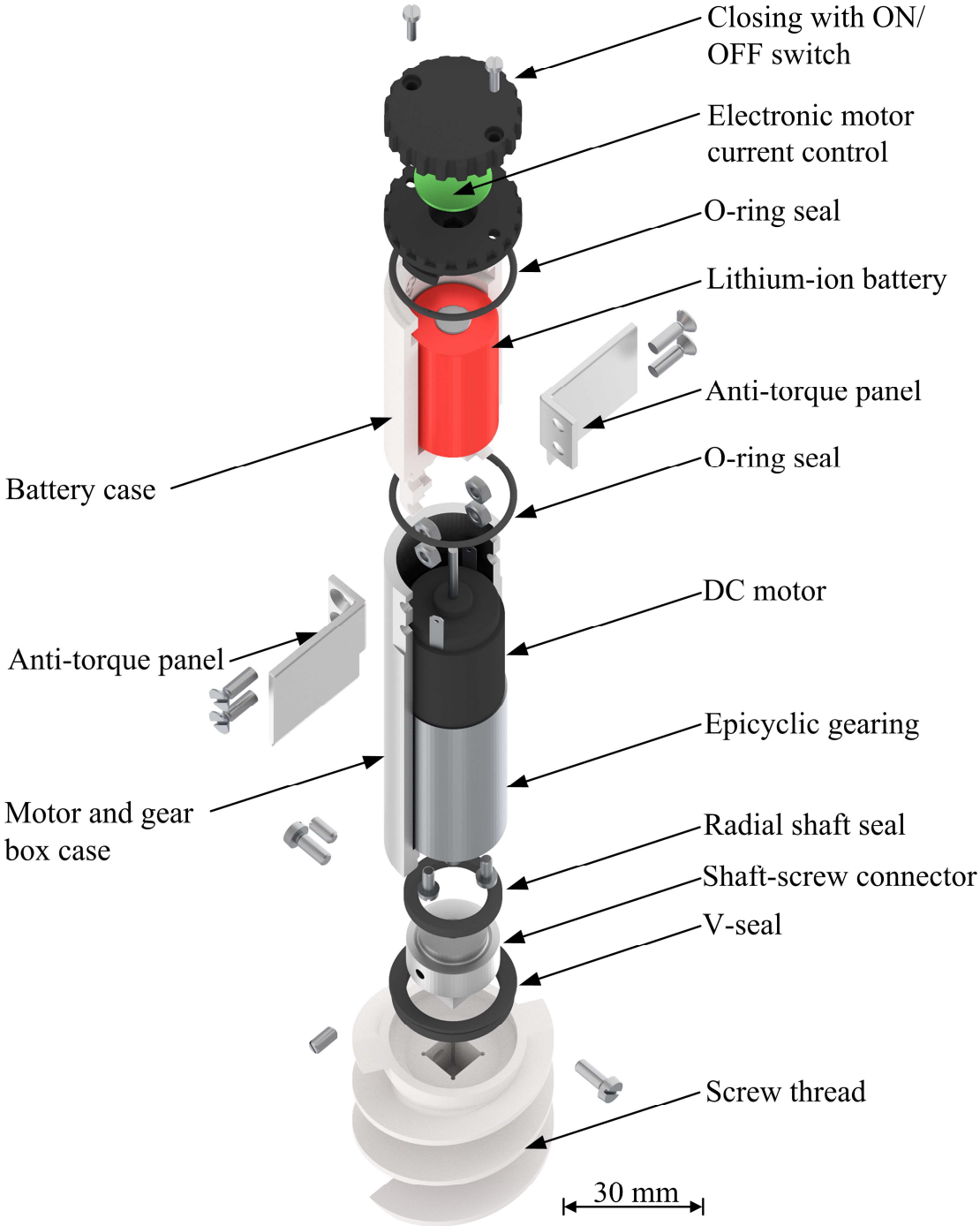

Figure 9: Exploded view of the prototype.

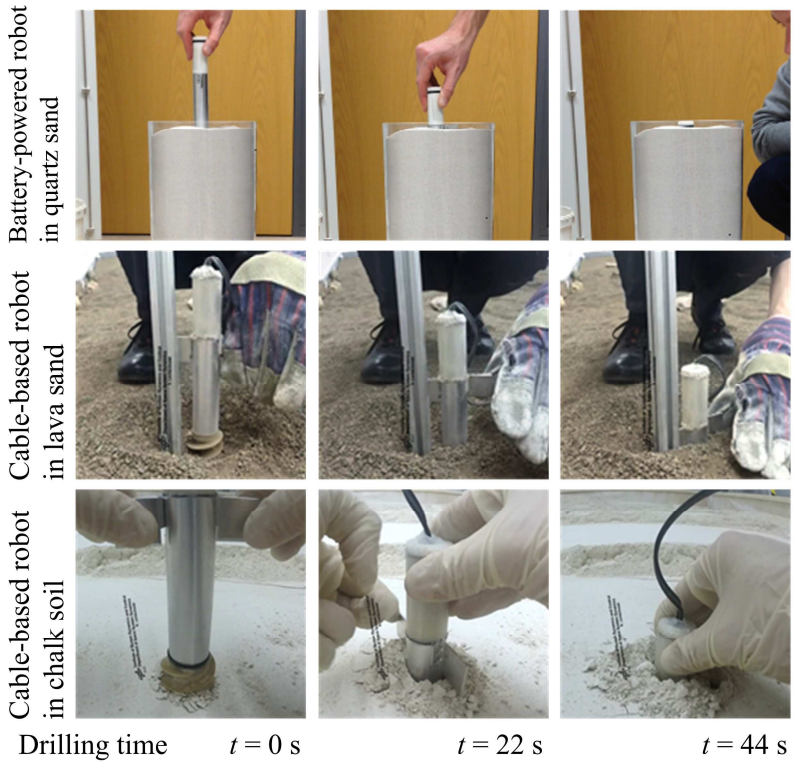

Figure 10: Drilling into different soils of the mobile robots with manual torque support - battery-powered robot and cable-based version.

6. CONCLUSIONS AND OUTLOOK

In this article an autonomous drilling robot for the locomotion in sandy soils alongside with a drilling performance testbed and approaches in modeling are presented. Using the designed testbed, first effects caused by diverse screw parameters are identified deploying two different types of screws. The use of the full robot in different soils enabled to successfully verify the locomotion and sealing concept. However, different than stated in literature, the maximum torque is not the only limiting factor for the locomotion and final penetration depth. Dependent on the actuator torque and screw design, the final depth is also limited by the shear strength of the surrounding soil. Thus, future development should be focused on reaching greater depth, while reducing the required torque and having a well-balanced distribution of the loads on the screw head.

However, to identify dedicated dependencies further parameters need to be investigated. Hence, such research will be part of future work in experiments and simulation. In order to enable the latter, a fully dynamic model, especially covering the driving forces of the screw head, will be developed.

REFERENCES

[1] L. Richter, P. Coste, V. Gromov, H. Kochan, S. Pinna, H. E. Richter, “Development of the ‘Planetary Underground Tool’ Subsurface Soil Sampler for the Mars Express ‘Beagle 2’ Lander,” in Advanced Space Research, vol. 28, no. 8, pp. 1225–1230, 2001.

[2] C. Stoker, A. Gonzales, J. Zavaleta, “Moon/Mars Underground Mole,” Proc. of NASA Science and Technology Conference (NSTC), June 19-21, 2007.

[3] Galileo Avionica S.p.A: “Instrumented Mole System Executive Summary,” Cod. MCSP-SA-GA-015, Available at: http:// sci.esa.int/science-e/www/object/doc.cfm?fobjectid=40498, last visit: 23.05.2017, 2006.

[4] J. Grygorczuk, M. Banaszkiewicz, A. Cichocki, M. Ciesielska, M. Dobrowolski, B. Kedziora, J. Krasowski, T. Kucinski, M. Marczewski, M. Morawski, H. Rickman, T. Rybus, K. Seweryn, K. Skocki, T. Spohn, T. Szewczyk, R. Wawrzaszek, Ł. Wisniewski, "Advanced Penetrators and Hammering Sampling Devices for Planetary Body Exploration," in Proc. of 11th Symposium on Advanced Space Technologies in Robotics and Automation (ASTRA), April 12-15, 2011.
[5] R. Lichtenheldt, B. Schäfer, O. Krömer, "Hammering beneath the surface of Mars – Modeling and simulation of the impact-driven locomotion of the HP3-Mole," in Proc. of 56th International Scientific Colloquium (IWK), Ilmenau, Germany, September 12-16, 2014.
[6] H. Hansen-Goos, M. Grott, R. Lichtenheldt, T. L. Hudson, T. Spohn, "Predicted Penetration Performance of the InSight HP3 Mole," Proc. of 45th Lunar and Planetary Science Conference, March 17-21, 2014.
[7] R. Abe, Y. Kawamura, K. Kamijima, K. Muramaki, "Performance Evaluation of Contra-Rotating Drill for DIGBOT," in Proc. of SICE Annual Conference, August 18-21, 2010, pp. 885–888.
[8] K. Nagaoka, T. Kubota, M. Otsuki, S. Tanaka, "Robotic Screw Explorer for Lunar Subsurface Investigation: Dynamics Modelling and Experimental Validation," in Proc. of IEEE International Conference on Robotics and Automation (ICRA), May 12-17, 2009.
[9] K. Nagaoka, "Study on Soil-Screw Interaction of Exploration Robot for Surface and Subsurface Locomotion in Soft Terrain," PhD thesis at Graduate University for Advanced Studies, Sodenkai, Japan, 2011.
[10] S. Yasuda, K. Komatsu, S. Tanaka, "Self-Turning Screw Mechanism for Burying Geophysical Sensors under Regolith," in Proc. of 11th International Symposium on Artificial Intelligence, Robotics and Automation in Space (ISAIRAS), September 4-6, 2012.
[11] Y. Bar-Cohen, M. Badescu, S. Sherrit, K. Zacny, G. Paulsen, L. Beegle, X. Bao, "Deep Drilling and Sampling via the Wireline Auto-Gopher Driven by Piezoelectric Percussive Actuator and EM Rotary Motor," in Proc. of Sensors and Smart Structures Technologies for Civil, Mechanical and Aerospace Systems, April 26, 2012.
[12] K. Zacny, G. Paulsen, Y. Bar-Cohen, L. Beegle, S. Sherrit, M. Badescu, B. Mellerowicz, O. Rzepiejewska, J, Craft, S. Sadick, F. Corsetti, Y. Ibarra, X. Bao, H. J. Lee, B. Abbey "Wireline Deep Drill for Exploration of Mars, Europa, and Enceladus," in Proc. of IEEE Conference on Aerospace, March 02-09, 2013, pp. 1–14.
[13] S. P. Gorevan, K. Y. Kong, T. M. Myrick, P. W. Bartlett, S. Sing, S. Stroescu, Roopnarine, S. Rafeek,"An Inchworm Deep Drilling System for Kilometer Scale Subsurface Exploration of Mars (IDDS)," in Proc. of Concepts and Approaches for Mars Exploration, (6095), July 18-20, 2000, pp. 129-130.
[14] S. P. Gorevan, T. M. Myrick, C. Batting, S. Mukherjee, P. Bartlett, J. Wilson, "Strategies for future Mars exploration: An infra-structure for the near and longerterm future exploration of the subsurface of Mars," in Proc. of 6th International Conference on Mars, (3196), July 20-25, 2003.
[15] C. Darukhanavala, A. Lycas, A. Mittal, A. Suresh, "Design of a Bimodal Self-Burying Robot," in Proc. of IEEE International Conference on Robotics and Automation (ICRA), 2013.
[16] J. Johnson, B. Sanders, C. Carmen, "Design and Development of a Ground Based Robotic Tunneling Worm for Operation in Harsh Environments," in Proc. of 62nd International Astronautical Congress, October 3-7, vol. 2(9954), 2011.

[17] H. Omori, T. Murakami, H. Nagai, T. Nakamura, T. Kubota, “Development of a Novel Bio-Inspired Planetary Subsurface Explorer,” in IEEE/ASME Transactions on Mechatronics, vol. 18, no. 2, 2013.
[18] H. Omori, “Development of Lunar or Planetary Sub-surface Exploration Robot Using Peristaltic Crawling,” PhD thesis at Graduate School of Science and Engineering, Chuo University, Tokyo, Japan, 2014.
[19] A. Fukunaga, J. M. Morookian, K. Quillin, A. Stoics, S. Thakoor, “Technical Support Package on Earthwormlike Exploratory Robots,” NASA Tech Brief, vol. 22, no. 6, 1998.
[20] Georgia Institute of Technology, “Heads Up, Robots: A Tiltable Head Could Improve the Ability of Undulating Robots to Navigate Disaster Debris,” Available at: http://www.gtresearchnews.gatech.edu/sandfish-robot/, last visit: 23.05.2017, 2011.
[21] A. G. Winter, R. L. H. Deits, D. S. Dorsch, A. H. Slocum, A. E. Hosoi, “Razor Clam to RoboClam: Burrowing Drag Reduction Mechanisms and their Robotic Adaption,” in Bioinspiration & Biomimetics, no. 9, 2014.
[22] R. A. Russell, “An Agile Burrowing Robot for Under-ground Chemical Source Location,” in Proc. of Australasian Conference on Robotics and Automation (ARAA), December 7-9, 2011.
[23] E. Susila, R. Hryciw, “Large displacement FEM modeling of the cone penetration test (CPT) in normally consolidated sand,” in International Journal for Numerical and Analytical Methods in Geomechanics, 27:585602, March 2003.
[24] W. Huang, D. Sheng, S. Sloan, H. Yu, “Finite element analysis of cone penetration in cohesionless soil,” in Computers and Geotechnics, (31):517528, September 2004.
[25] J. Grygorczuk, K. Seweryn, R. Wawrzaszek, M. Banaszkiewicz, ”Technological Features in the new Mole Penetrator ‘KRET’," in Proc. of 13th European Space Mechanisms and Tribology Symposium (ESMATS), September 23-25, 2009.
[26] R. Lichtenheldt, O. Krömer, “Soil Modeling for InSight's HP3-Mole: From Highly Accurate Particle-Based Towards Fast Empirical Models,” in Proc. ASCE Earth and Space Conference, April 11-15, 2016.
[27] K. Terzaghi, R. Peck, G. Mesri, “Soil Mechanics in Engineering and Practice”, John Wiley & Sons, Inc., 1996.
[28] H. Türke, Statik im Erdbau, Ernst und Sohn, Berlin, 1999.
[29] R. Salgado, J. Mitchell, “Cavity Expansion and Penetration Resistance in Sand”, Journal of Geotechnical and Geoenvironmental Engineering, pp- 344–354, 1997.
[30] R. Salgado, J. Mitchell, M. Jamilokowski, “Calibration Chamber Size Effects on Penetration Resistance in Sand”, Journal of Geotechnical and Geoenvironmental Engineering, pp. 878–888, 1998.
[31] T. Whitaker, The Design of Piled Foundations, Pergamon Press, 2nd edition, 1976.
[32] R. Lichtenheldt, „Hammering beneath the Surface of Mars - Analyse des Schlagzyklus und der äußeren Form des HP3-Mole mit Hilfe der Diskrete Elemente Methode“, IFToMM D-A-CH, Dortmund, ISBN 978-3-940402-03-5, 2015.
[33] F. Becker, S. Börner, R. Lichtenheldt, K. Zimmermann, „Enabling Autonomous Locomotion into Sand – A Mobile and Modular Drilling Robot,” in Proc. of Int Symposium on Robotics (ISR), June 21-22, 2016, VDE Verlag, pp. 307–312.

CONTACTS

Dr.-Ing. R. Lichtenheldt roy.lichtenheldt@dlr.de
Dr.-Ing. F. Becker felix.becker@tu-ilmenau.de
Univ.-Prof. Dr.-Ing. habil. K. Zimmermann klaus.zimmermann@tu-ilmenau.de